Journal of the Mechanics and Physics of Solids 105 (2017) 81–94

Contents lists available at ScienceDirect

Journal of the Mechanics and Physics of Solids

journal homepage: www.elsevier.com/locate/jmps

High-performance electromechanical transduction using laterally-constrained dielectric elastomers part I: Actuation processes

Soo Jin Adrian Koh[a,*], Christoph Keplinger[b,c,d], Rainer Kaltseis[e], Choon-Chiang Foo[f], Richard Baumgartner[e], Siegfried Bauer[e], Zhigang Suo[b]

[a] National University of Singapore, Department of Mechanical Engineering and Engineering Science Programme, 9 Engineering Drive 1, Singapore 117575, Singapore
[b] Harvard University, Kavli Institute for Nanobio Science and Technology, School of Engineering and Applied Sciences, Cambridge, MA 02138, USA
[c] Department of Mechanical Engineering, University of Colorado, Boulder, CO 80309, USA
[d] Materials Science and Engineering Program, University of Colorado, Boulder, CO 80309, USA
[e] Johannes-Kepler University, Soft-Matter Physics, Linz A-4040, Austria
[f] Institute of High Performance Computing, 1 Fusionopolis Way, #16-16, Connexis North, Singapore 138632, Singapore

ARTICLE INFO

Article history:
Received 15 December 2016
Revised 21 March 2017
Accepted 22 April 2017
Available online 10 May 2017

ABSTRACT

A dielectric elastomer transducer is a deformable capacitor, and is under development as a sensor, actuator, or generator. Among various geometric configurations, laterally-constrained transducer, also known as pure-shear transducer, is easy to implement and effective to couple mechanical force and electrical voltage. This analytical study reveals that lateral pre-stretch enhances actuation, far exceeding previously reported actuation strokes. Laterally-constrained transducers exhibit complex electromechanical behavior. As voltage increases, an actuator may undergo electromechanical instability, or form wrinkles, or suffer electrical breakdown. We survey the behavior of actuators under all possible states of pre-stretches, and identify five modes of actuation. Our analysis predicts that laterally-constrained actuators can achieve actuation stroke of 1000% for an acrylic elastomer, and 230% for natural rubber. This analysis opens the door to design actuators of simple geometry capable of a very large range of electromechanical actuation.

1. Introduction

Electroactive polymers (EAPs) are on the verge of commercialization, yet their theoretical base is still incomplete due to diverse physical principles of transduction, types of materials, as well as geometric configurations of transducers. One particular class of EAP is the dielectric elastomer (DE). A DE transducer consists of a thin membrane of elastomer, sandwiched between two compliant electrodes. Subject to voltage, electric charges of the opposite polarities accumulate on the two faces of the membrane, and the membrane reduces its thickness and expands its area. The voltage causes a change in

* Corresponding author.
E-mail address: adrian_koh@nus.edu.sg (S.J.A. Koh).

http://dx.doi.org/10.1016/j.jmps.2017.04.015
0022-5096/

shape; the DE functions as an actuator (Pelrine et al., 2000; Plante and Dubowsky, 2007; Carpi et al., 2010; Koh et al., 2011; Keplinger et al., 2012; Huang et al., 2012; Lu et al., 2014; An et al., 2015), resembling a muscle. A charged DE membrane changes its capacitance with mechanical deformation. The change in capacitance due to mechanical deformation allows the DE to function as a sensor, much like the human skin (Carpi and De Rossi, 2005; Kasahara et al., 2011; Gisby et al., 2013; Kim et al., 2013; Laflamme et al., 2013; Böse and Fuβ, 2014). A charged DE may also be cyclically stretched and relaxed, which allows electrical charges to be pumped from a low voltage source to a high voltage reservoir. The charges may then be stored at high voltage, or directly released to power an electrical load. In this case, the DE functions as a stretchable generator of electrical energy (Pelrine et al., 2001; Koh et al., 2009; Huang et al., 2013; McKay et al., 2010; Kaltseis et al., 2014; McKay et al., 2015).

Mechanical force can stretch a membrane in any direction, but electrical voltage tends to thin down the membrane and expands it equally in all its in-plane directions. The combined mechanical force and electrical voltage result in a rich and interesting range of electromechanical responses.

The mechanical response of a membrane is often studied based on three modes of deformation: uniaxial, equal-biaxial, and laterally-constrained (also known as "pure shear") (Treloar, 1975). In uniaxial deformation, only one direction is subject to mechanical stress. In equal-biaxial deformation, two directions are subject to equal mechanical stress. In the laterally-constrained deformation, the membrane is constrained from deforming in one planar direction, and is pulled by a mechanical force in a direction perpendicular to the constrained direction.

Fundamentally, a DE expanding unconstrained under an electric field expands in the mode of equal-biaxial deformation. The more the electric field dominates the actuation the more the deformation approaches an equal-biaxial mode of deformation, which allows for simplifying the deformation for analysis and design. Due to the simplicity of this mode of deformation, many analytical studies have been performed (Zhao and Suo, 2007; Zhao et al., 2007; Koh et al., 2011; Kollosche et al., 2015) on both the actuator and the generator modes of operation. It has also been shown analytically that one may extract the maximal amount of energy from equal-biaxial deformation (Koh, 2009). An analytical study demonstrates that the maximum actuation strain for a DE under uniaxial pre-stretch always fails by electromechanical instability (EMI), achieving actuation strains of less than 30% (Huang and Suo, 2011). On the other hand, a DE pre-stretched equal-biaxially has exhibited actuation strains beyond 300% in areal expansion (Pelrine et al., 2000; Keplinger et al., 2012; Huang et al., 2012). It is also possible to harness EMI so that an unprecedented 1692% areal expansion may be achieved (Keplinger et al., 2012).

While both theory and experiments have demonstrated that the equal-biaxial mode maximizes performance of a DE, to operate a DE in equal-biaxial mode is challenging. Although the uniaxial mode offers a simpler method of operation, its performance is inferior compared to the equal-biaxial mode. Here we study a laterally-constrained DE (Fig. 1). In this configuration, a rectangular-shaped DE membrane is clamped on the long edges. Pre-stretch may first be applied along the long edges prior to clamping, giving lateral pre-stretch λ_{2p} (Fig. 1b). Application of mechanical force P gives rise to longitudinal pre-stretch λ_{1p} (Fig. 1b). The DE is constrained from expanding in the clamped lateral direction, but is free to deform in the longitudinal direction (Fig. 1c). In our analysis, we idealize that the DE is fully constrained in the lateral direction, so that λ_{2p} is a constant during deformation. In reality, regions away from the edge clamps are free to deform with mechanical and electrical loading. The objective of our analysis is to analyze a particular class of idealized deformation mode, known as the "pure shear" or plane strain mode, commonly studied in polymer physics (Treloar, 1975). One may replicate this idealized clamped mode by clamping a membrane with high aspect ratio, along its long edge. In fact, experiments have shown that, for large aspect ratios of 3 or more, appropriate lateral pre-stretch allowed the DE to attain an electrically-actuated strain of 260% (Kollosche et al., 2012). While the performance of a laterally-constrained DE has been studied as an actuator, the results are incomplete for two reasons. First, discrete values of pre-stretches studied in current literature may not reveal all possible modes of actuation in a laterally-constrained DE. Second, the maximum amount of energy that may be converted for a laterally-constrained DE has not been analyzed. This study on laterally-constrained DE is motivated by previous works showing large actuation of a laterally-constrained DE, while retaining a simple mode of operation (Kollosche et al., 2012; Zhu et al., 2012).

We present a theoretical analysis of a laterally-constrained DE. This configuration is simple to construct, but the electromechanics and physics of operation are complex. The magnitude and combination of pre-stretches (λ_{1p}, λ_{2p}) determines how the DE actuates. Subject to an increasing electric field, the DE may actuate with a flat membrane, or actuate with a wrinkled membrane. As the electric field increases, the stress along the lateral, clamped direction is relaxed. At a sufficiently high field, due to the competing effects of a constrained membrane and Maxwell stress from electric field, the membrane may lose lateral tension. As the electric field continues to increase, compressive stresses due to increasing Maxwell stress in the constrained membrane will cause wrinkles to develop – the DE transits from a flat to a wrinkled state. The analysis reveals five modes of actuation, depending on the combination of pre-stretches (λ_{1p}, λ_{2p}). We show that an appropriate level of lateral pre-stretch greatly enhances the magnitude of electrical actuation, far exceeding previously reported actuation strokes. Our analysis predicts that laterally-constrained actuators can achieve actuation stroke of 1000% for the acrylic elastomer, and 230% for natural rubber. In part II of a paper bearing the same title, we will further show that lateral pre-stretch allows a DE to convert energy comparable to the equal-biaxial mode of deformation, while retaining a simple mode of uniaxial deformation. A DE operating in this mode may be easily modularized, and be integrated in robotic systems or energy harvesting devices as high performance electromechanical transducers.

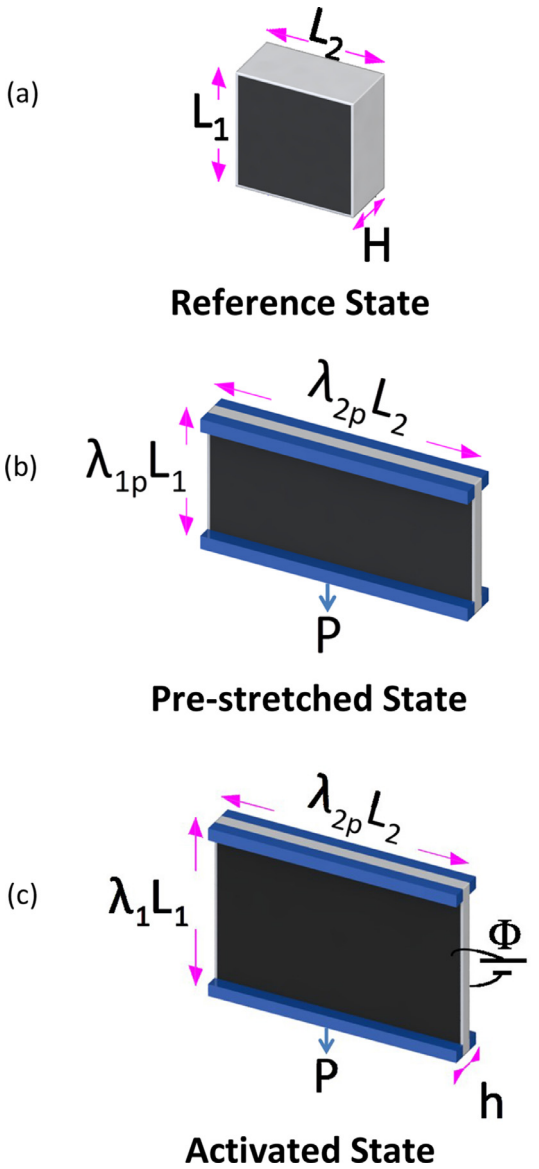

Fig. 1. States of a laterally-constrained dielectric elastomer actuator. (a) In the reference state, the membrane is unstressed and uncharged. (b) In a pre-stretched state, the membrane is pre-stretched and clamped in its lateral direction, and is subject to a force $\boldsymbol{P}$ to pre-stretch the membrane in the vertical direction. (c) In an activated state, the membrane is subject to the force $\boldsymbol{P}$ and a voltage $\boldsymbol{\Phi}$.

2. A dielectric elastomer subject to voltage and forces

This section reviews the basic theory of a dielectric elastomer subject to voltage and forces (Suo, 2010). We define an unstretched and uncharged DE as the reference state (Fig. 1a). At this state, the dimensions of the DE membrane are L_1, L_2 and H. A stretched and charged DE deforms to dimensions of l_1, l_2 and h, which we term the activated state. We define the principal stretches as follows: $\lambda_1 = l_1/L_1$, $\lambda_2 = l_2/L_2$, $\lambda_3 = h/H$. Assuming incompressibility, we write: $\lambda_3 = \lambda_1^{-1}\lambda_2^{-1}$. In developing the basic theory, we assume that the DE is subject to constant forces P_1 and P_2 in the plane, and constant voltage across the thickness Φ. The DE, the weights that apply the forces and battery that applies the voltage, together constitute a composite system. We further assume the model of ideal dielectric elastomer – that is, the DE is a linear dielectric, and the permittivity ε is independent of deformation. Thus, the electric displacement D is linear in the electric field E: $D = \varepsilon E$. Recall that $\Phi = Eh$, and the charge Q on the dielectric relates to the electric displacement as $Q = Dl_1l_2$, so that the charge relates to the voltage as $Q = \varepsilon(\Phi/H)L_1L_2\lambda_1^2\lambda_2^2$. Because the DE is a deformable capacitor, the deformation affects the charge-voltage

relation. The Helmholtz free energy of this composite system is a function of two stretches, $F(\lambda_1, \lambda_2)$, given by:

$$\frac{F(\lambda_1,\lambda_2)}{L_1L_2H} = W_s(\lambda_1,\lambda_2) - \frac{P_1}{L_2H}\lambda_1 - \frac{P_2}{L_1H}\lambda_2 - \frac{1}{2}\varepsilon\left(\frac{\Phi}{H}\right)^2\lambda_1^2\lambda_2^2 \tag{1}$$

where $W_s(\lambda_1, \lambda_2)$ is the free-energy density of deformation for the elastomer, where we pre-suppose that the first variation was carried out on a linear, ideal dielectric, given by Eq. (2c) below. Integrating both sides of (2c) with respect to (Φ/H) gives (1). At equilibrium the free energy F is minimal and thus remains constant upon small variation of the internal variables λ_1 and λ_2: $\partial F/\partial\lambda_1 = \partial F/\partial\lambda_2 = 0$. This minimization leads to:

$$\frac{P_1}{L_2H} + \varepsilon\left(\frac{\Phi}{H}\right)^2\lambda_1\lambda_2^2 = \frac{\partial W_s}{\partial\lambda_1} \tag{2a}$$

$$\frac{P_2}{L_1H} + \varepsilon\left(\frac{\Phi}{H}\right)^2\lambda_1^2\lambda_2 = \frac{\partial W_s}{\partial\lambda_2} \tag{2b}$$

We also list the relation between the charge and voltage:

$$\frac{Q}{L_1L_2} = \varepsilon\left(\frac{\Phi}{H}\right)\lambda_1^2\lambda_2^2 \tag{2c}$$

Once $W_s(\lambda_1, \lambda_2)$ is defined, the state of a DE is completely described by mechanical forces P_1, P_2, mechanical stretches λ_1, λ_2, voltage Φ, and charge Q. Equation (2) describes a system of three degrees of freedom; one may independently prescribe any three quantities, and solve for the other three.

To define $W_s(\lambda_1, \lambda_2)$, we select a simple material model that captures two essential characteristics of a covalently cross-linked elastomer: small-strain neo-Hookean elasticity, and divergence of free energy when polymer chains approach their contour lengths. We adopt the Gent model (Gent, 1996):

$$W_s(\lambda_1,\lambda_2) = -\frac{\mu J_{\lim}}{2}\ln\left(1 - \frac{\lambda_1^2+\lambda_2^2+\lambda_1^{-2}\lambda_2^{-2}-3}{J_{\lim}}\right) \tag{3}$$

where μ is the small-strain shear modulus, $J_{\lim}$ is a dimensionless parameter that defines the limiting stretch. When the deformation is small compared to the limiting stretch, $(\lambda_1^2+\lambda_2^2+\lambda_1^{-2}\lambda_2^{-2}-3)/J_{\lim} \to 0$, a Taylor expansion of (3) recovers the free-energy density function for an incompressible elastomer with neo-Hookean elasticity. When the deformation approaches the limiting stretch $(\lambda_1^2+\lambda_2^2+\lambda_1^{-2}\lambda_2^{-2}-3) \to J_{\lim}$, the stretch-related free energy density $W_s(\lambda_1, \lambda_2)$ diverges.

Equations (2) and (3) give the equations of state for a dielectric elastomer. $J_{\lim}$ in Eq. (3) imposes a physical limit to the stretches that may be applied on the elastomer. In this study, we prescribe $J_{\lim} = 125$ – a representative value for the commonly-used, acrylic-based VHB elastomer (Huang et al., 2012; Kaltseis et al., 2014), and $J_{\lim} = 50$ – a representative value for natural rubber (Kaltseis et al., 2014; Koh et al., 2011).

The stretch limits implicitly assume a polymer with infinite fracture strength. This is not realistic. The maximum stretch of a polymer is usually governed by its fracture strength, which limits the maximum stretch of a polymer to be smaller than that stipulated by $J_{\lim}$. In this paper, we seek to understand the qualitative characteristics of a laterally-constrained DE and not the numerical limits of its performance; we therefore impose a maximum stretch of 95% of the limiting stretch defined by $J_{\lim}$. This maximum stretch was assumed for convenience of analysis.

3. Electrically-induced actuation response in laterally-constrained dielectric elastomers

To specialize Eqs. (1–3) for a laterally-constrained DE, we prescribe lateral pre-stretch $\lambda_2 = \lambda_{2p}$. We define the pre-stretched state in Fig. 1b. Assuming incompressibility, lateral pre-stretch (λ_{2p}) causes the stretch in the longitudinal (λ_1) direction to contract in accordance with $\lambda_1 = \lambda_{2p}^{-1/2}$. A mechanical force P may then be applied in the longitudinal direction, to induce pre-stretch λ_{1p}. When voltage is applied, the DE deforms in the λ_1 direction (Fig. 1c). Here, we study actuation of the DE membrane under a fixed load $P = P_{\text{dead}}$. Hence, for a specific combination of $(\lambda_{1p}, \lambda_{2p})$, one may expect a unique actuation response to voltage. Scanning the entire $(\lambda_{1p}, \lambda_{2p})$ space will reveal a broad range of actuation responses.

For a laterally-constrained membrane with $\lambda_2 = \lambda_{2p}$ and a fixed load P_{dead}, as the voltage increases, the lateral nominal stress s_2, given by P_2/L_1H in Eq. (2b), will reduce. One may confirm this mathematically by inspecting Eq. (2b), and setting $\lambda_2 = \lambda_{2p}$. As long as $P_2 > 0$, the lateral stretch is preserved at the prescribed λ_{2p}. At a sufficiently high voltage, the lateral stress will be completely relaxed (that is, $P_2 = 0$). The magnitude of this voltage may be predicted by setting $P_2 = 0$ and $\lambda_2 = \lambda_{2p}$ in Equation (2), and solve for Φ and λ_1 simultaneously. We mark this point of transition with a square (point C in Fig. 2 and several curves in Fig. 4). Further increase in voltage beyond this will result in the DE actuating with no lateral mechanical stress, similar to that of uniaxial deformation (Zhu et al., 2012). An increasing electric field thus causes the lateral stretch to increase by virtue of Maxwell stress. However, due to constraints provided by the clamps in the laterally-constrained configuration, increase in lateral stretch causes the DE membrane to develop wrinkles. Hence, even though actuation under a uniaxial load is similar, in terms of the states of stress, to a laterally-constrained DE after it loses lateral

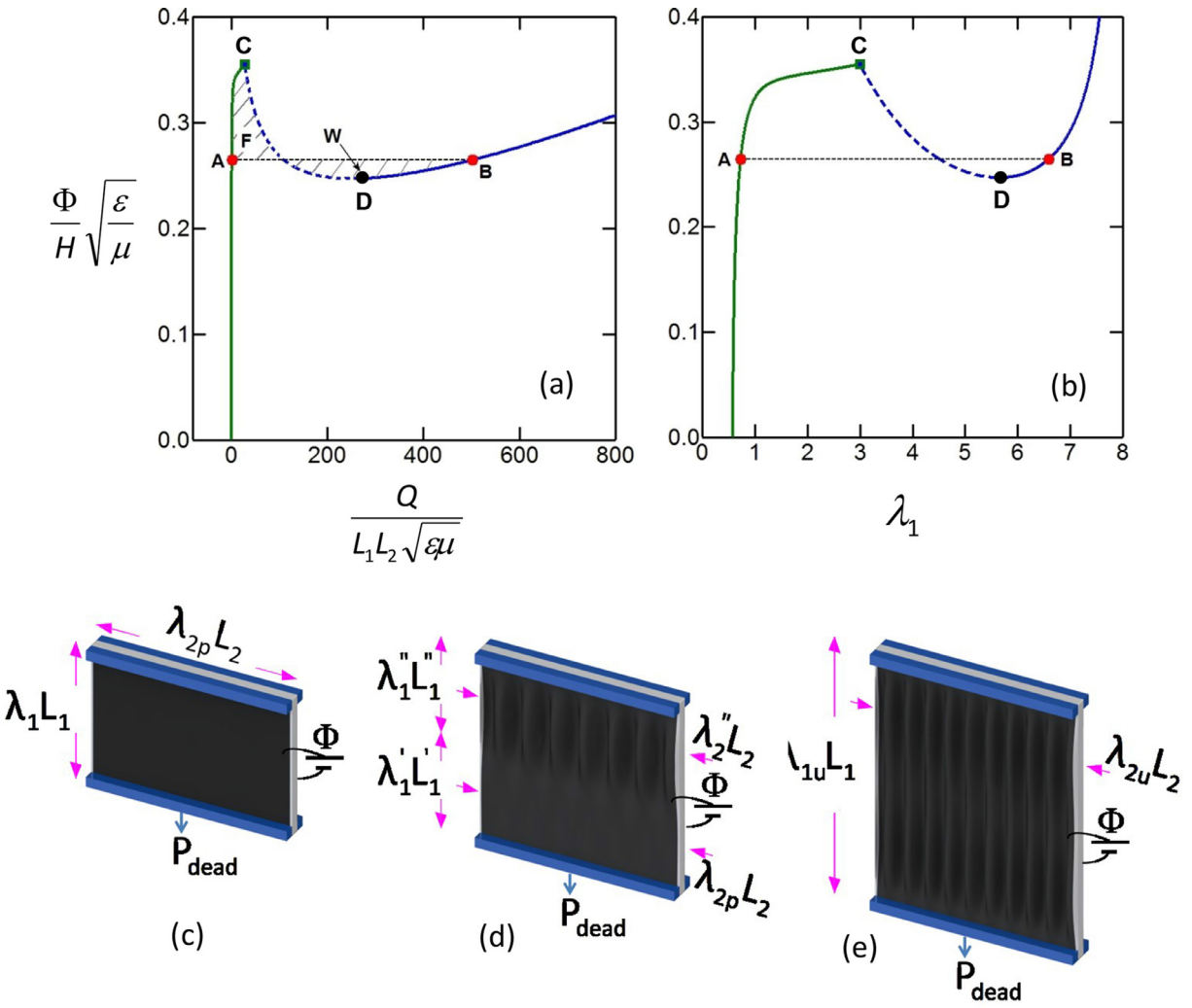

Fig. 2. Non-monotonic electromechanical response, leading to electromechanical instability and transition of states. Using an example of a dielectric elastomer (DE) with $J_{\text{lim}} = 125$ and $\lambda_{2p} = 3$, with no dead load ($\lambda_{1p} = 3^{-1/2}$, $\mathbf{P_{dead}} = 0$): (a) Response on a voltage-charge work conjugate plot, showing the Maxwell construction for phase transition, indicated by line **AB**; (b) Response on the voltage-stretch plot, with the same transition path **AB**; (c) Geometry of DE in the flat, low charge/stretch state; (d) Geometry of DE with co-existent phases – a state on the transition path **AB**; (e) Geometry of DE in the wrinkled, high charge/stretch state beyond **B**.

tension, they differ in terms of its deformed geometry. Here, we assume that the curvature of the wrinkles is small and analyze a wrinkled laterally-constrained membrane like that of a flat uniaxially-deformed membrane. To do this, we set $P_2 = 0$ in Eq. (2b), prescribe a voltage and solve for λ_1 and λ_2 simultaneously from (2). Subsequent response beyond lateral tension loss is shown as a blue line in Figs. 2, 3 and 4.

The discussion above avoided a conspicuous phenomenon – electromechanical instability (EMI). Physically, EMI refers to the critical voltage where positive feedback ensues between a thinning membrane and an increasing electric field. It is well-known that EMI takes place in a DE that is deformed equal-biaxially and uniaxially Zhao and Suo, 2007; Huang and Suo, 2011). Mathematically, this condition is represented as a non-positive-definite Hessian of the free energy (Zhao and Suo, 2007). One may then prove, from Eqs. (2) and (3), that EMI does not take place when the DE is laterally-constrained. However, when the voltage is large enough to cause the lateral stress to be fully relaxed, the DE ceases to deform in a laterally-constrained mode, but in the uniaxial mode. EMI may then take place, in a similar fashion as that in uniaxial deformation [Huang and Suo, 2011, Zhu et al., 2012 and Fig. 2].

We note that the voltage required to relax a DE membrane to a laterally stress-free state will vary with the combination of pre-stretches applied in both directions (λ_{1p}, λ_{2p}). Note here that λ_{1p} may be read off from the horizontal axis at $\Phi = 0$ and is caused by the fixed load P_{dead} (Fig. 2b and Fig. 4). For a laterally-constrained DE with no pre-stretch in any direction ($\lambda_{1p} = \lambda_{2p} = 1$, Fig. 4a), the DE immediately loses tension once voltage is applied, and actuates purely in a fashion similar to the equal-biaxial mode.

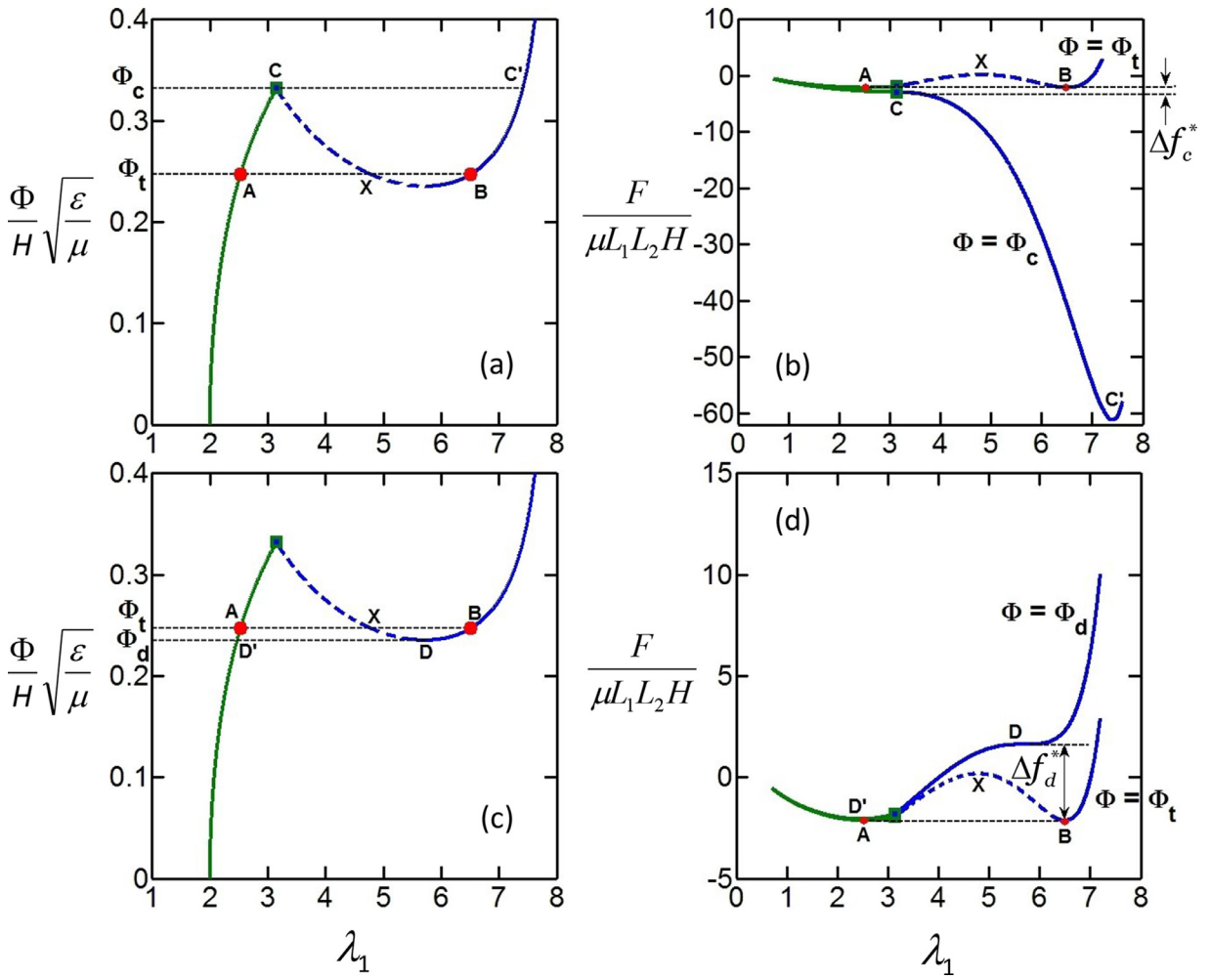

Fig. 3. Phase transition of a laterally-constrained dielectric elastomer (DE). The DE takes on two phases of low charge/stretch, and high charge/stretch. Solid lines indicate the energetically-stable states, while dashed lines indicate the energetically-unstable states in the equations of state (a, c) and the Helmholtz free energy (b, d).

Let the limiting stretch for equal-biaxial deformation be λ_{BI}, which is determined by solving the equation $2\lambda_{BI}^2 + \lambda_{BI}^{-4} - 3 = J_{\lim}$. For a constrained DE laterally pre-stretched beyond the limiting stretch for equal-biaxial deformation, $\lambda_{2p} > \lambda_{BI}$, lateral loss of tension will not occur at any level of voltage. Such a highly pre-stretched membrane may achieve very large actuation (Fig. 4d).

One may also note, from Figs. 4a–c, when $\lambda_{1p} > \lambda_{BI}$, denoted by the lines lying rightmost on each plot, the DE first exhibits an electromechanically-stiff response when $s_2 > 0$ (green lines), then contracts with increasing voltage after $s_2 < 0$ (blue lines). This phenomenon resembling natural muscles is a unique feature for DEs stretched in a uniaxial manner (Huang and Suo, 2011). Any lateral pre-stretches smaller than λ_{BI} give varied electromechanical responses, with the DE generally transiting from a flat, laterally-constrained state (green line), to a wrinkled state (blue line), with the filled square marker denoting the point of transition. We will classify different classes of electromechanical response in a subsequent section.

4. Electromechanical instability and phase transition

Electromechanical instability (EMI) manifests in a DE system if the system becomes energetically unstable – a small change in voltage or force (intensive field variables) will lead to a runaway change in the state of charge or stretch (extensive field variables). In general, when a physical system undergoes instability, a small change in the intensive field variable will lead to an extreme change in the corresponding extensive field variable. One example is the melting of ice, whereby a small change in temperature (intensive) in the vicinity of 0°C, causes to a huge change in entropy (extensive), leading to a first-order phase transition from ice (solid), to water (liquid). Another example is the necking of an iron bar when, at a state of

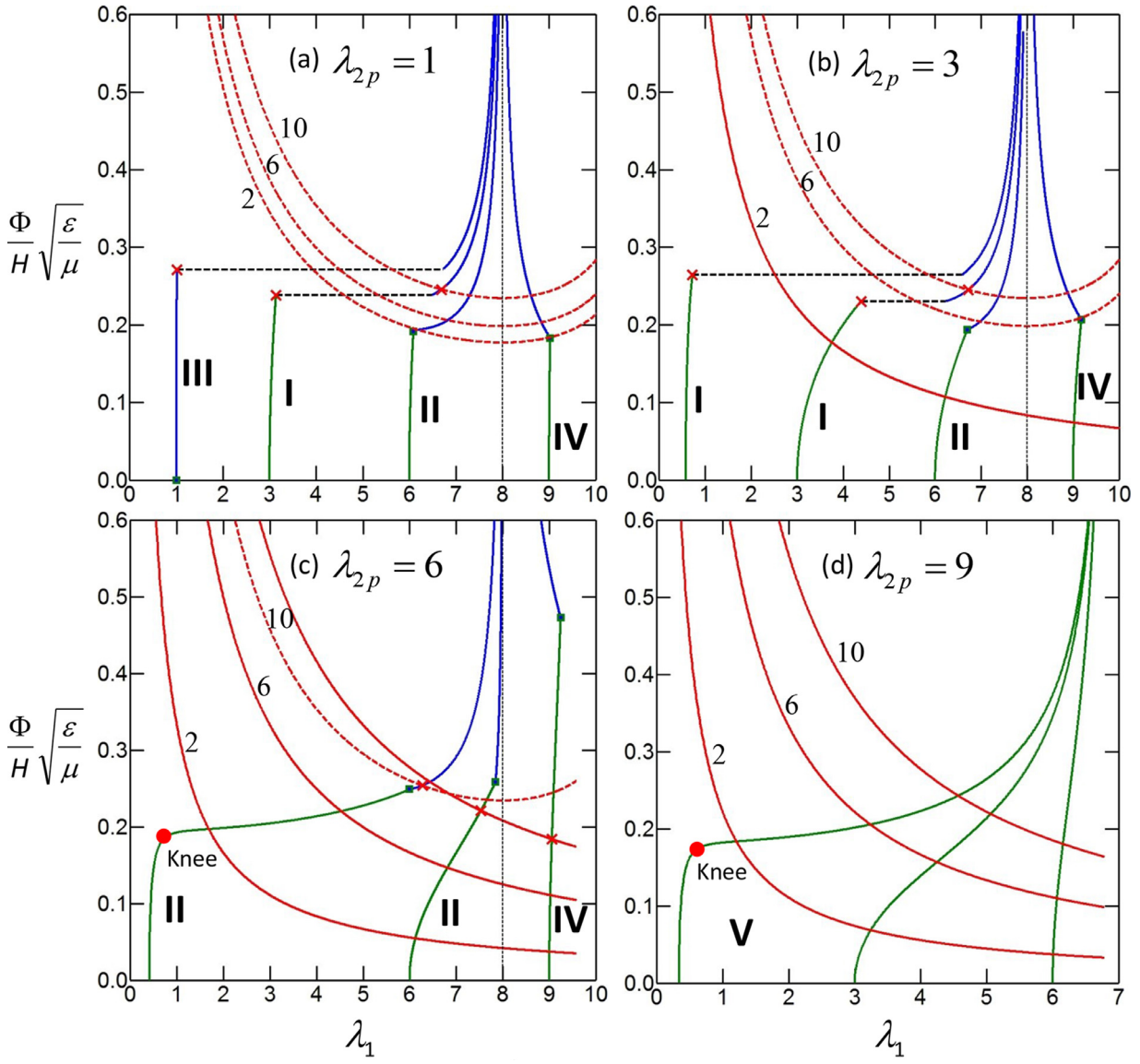

Fig. 4. Voltage-stretch curves for laterally-constrained actuators ($J_{lim}=125$) with various levels of pre-stretches and electrical breakdown strengths in flat (green) and wrinkled (blue) states. The five modes of actuation, **I, II, III, IV** and **V** are described in Section 5 and Table 1. Breakdown strengths E_B (red lines) determine an upper limit to operating voltage and the maximum electrically actuated stretch of the actuator. Solid red lines denote breakdown curves for flat states. Dashed red lines refer to the breakdown limit in wrinkled states (equivalent uniaxial configuration). Numbers on the breakdown curves indicate a factor given by a combination of material properties $E_{EB}\sqrt{\epsilon/\mu}$. Very large electrically-induced actuation is possible at the voltage denoted by red solid circular markers on (c) and (d), marked by "Knee", beyond which actuation becomes very sensitive to small increase in voltage. All voltage-stretch curves in (d) belong to mode **V** actuation. (For interpretation of the references to color in this figure legend, the reader is referred to the web version of this article.)

large tensile stress, a small change in the uniaxial force (intensive), leads to a large increase in its displacement (extensive), often rupturing the bar. In all instances, instability leads to huge change in the extensive field variable.

Following the equations of state listed in Equation (2), we plot the voltage–charge and voltage–stretch response (Fig. 2). For a voltage smaller than point **D** and higher than zero voltage, only one stable state exists. For a voltage between **D** and **C**, three states exist. Two of these states are thermodynamically stable (minima of the Helmholtz free energy), and one is unstable (maxima of the Helmholtz free energy). The range of unstable states is denoted by a dashed line, between **C** and **D**. The DE may undergo transition from a state of low charge and stretch, to a state of high charge and stretch at any voltages between **C** and **D**. The voltage level for transition depends on the density of nucleation sites in the DE. The nature of these nucleation sites may be regions of defects, imperfections, voids or inclusions/impurities. Phase transition begins at these nucleation sites, and gradually grows and dominates the entire system with the new phase. This process is termed

Table 1
Wrinkle formation and various modes of transition.

	How wrinkles appear	Evolution of stretch/charge with continuous control of voltage	Examples
Mode–I	*Gradual* (Fig. 2c→2d→2e)	*Discontinuous jump* at transition, membrane goes from flat to wrinkled at transition	Fig. 2a & b Fig. 3a & 3c Fig. 4a & 4b labelled with "I"
Mode–II	*Sudden* (Fig. 2c→2e)	*Continuous evolution*, no discontinuous jump at transition	Fig. 4a–c labelled with "II"
Mode–III	*Sudden* (Fig. 2c→2e)	*Discontinuous jump* at transition, membrane wrinkles before transition	Fig. 4a, labelled with "III"
Mode–IV	*Sudden* (Fig. 2c→2e)	*Continuous evolution*, no discontinuous jump at transition, accompanied by stretch reversal	Fig. 4a–c, labelled with "IV"
Mode–V	*No wrinkles* (Fig. 1c or 2c)	*Continuous evolution*, no wrinkles	Fig. 4d

heterogeneous nucleation. For a DE actuating under voltage control, the new phase is a state of high charge/high stretch. DE regions which are locally thinner contain microscopic air voids or impurities like conductive particles. Such nucleation sites lead to concentration of electric field and mechanical stress and localized phase transition takes place before the rest of the DE does so. These localized regions of new phases will grow at the expense of neighboring regions, gradually dominating the entire system with the new phase. This is the well-known mechanism of nucleation and growth, which the reader may refer to other references for a deeper discussion on these topics (Debenedetti and Stanley, 2003; Pruppacher and Klett, 2010).

For a DE with randomly-distributed nucleation sites, phase transition will take place at a voltage level following the Maxwell rule. The Maxwell rule is a construction on a work-conjugate plot, which states the level of intensive variable that causes phase transition, is a level that results in the two stable states of extensive variables with equal energy. Graphically, this construction is shown in Fig. 2a, whereby line **AB** denotes the transition voltage Φ_t, such that areas **F** and **W** are equal. A corresponding plot in the voltage–stretch plane is shown in Fig. 2b. Physically, two phases of low charge and stretch and high charge and stretch co-exist at Φ_t. Such a state of co-existence is transient. Fig. 2c–e shows schematics of a flat state (low charge/stretch), the co-existent state during transition, and a wrinkled state (high charge/stretch). Mathematically, one may express the state of co-existence by equating the Helmholtz free energy of the flat and wrinkled state (Eq. 1):

$$W\left(\lambda'_1,\lambda_{2p}\right)-\frac{P_{\text{dead}}}{L_2H}\lambda'_1-\frac{\varepsilon}{2}\left(\frac{\Phi_t}{H}\right)^2\left(\lambda'_1\lambda_{2p}\right)^2=W\left(\lambda''_1,\lambda''_2\right)-\frac{P_{\text{dead}}}{L_2H}\lambda''_1-\frac{\varepsilon}{2}\left(\frac{\Phi_t}{H}\right)^2\left(\lambda''_1\lambda''_2\right)^2 \tag{4}$$

whereby stretches λ'_1, λ''_1, λ''_2 are solved from the equations-of-state (2). Detailed derivation and solution for Φ_t are available in (Huang and Suo, 2011; Kollosche et al., 2012; Zhu et al., 2012).

The Maxwell rule suggests that phase transition occurs at a specific magnitude of the intensive variable. This is true for the melting of ice, as impurities in water are largely randomly-distributed, allowing water to undergo first-order transition at 0°C. On the other hand, phase transition may take place over a range of magnitudes, for instance, the necking stress in an iron bar, where location and density of defects in a bar is more diverse. In a particular instance, a system may be so pure, that no nucleation sites exist. Such a system will need to overcome an energy barrier to initiate nucleation, before phase transition could take place. This process is known as homogeneous nucleation. Naturally, homogeneous nucleation will require more energy to activate the process of phase transition, as compared to heterogeneous nucleation. Consequently, pure water may be supercooled, and remain in its liquid phase even below –40°C, or superheated before it turns into vapor at 374°C (Pruppacher and Klett, 2010). Analogously, a carefully manufactured DE membrane free from defects may be super-charged up to point **C**, before undergoing an instantaneous transition to **C'** (Fig. 3a). The super-charging voltage is Φ_c, given in Fig. 3a, and the energy barrier required to initiate phase transition in the DE membrane is given as Δf_c^* in Fig. 3b. Similarly, the same membrane may be super-discharged down to **D**, and then undergo a reverse transition to **D'** (Fig. 3c). The super-discharging voltage is given as Φ_d in Fig. 3c, with the energy barrier to initiate reverse phase transition as Δf_d^* in Fig. 3d. In Fig. 3, **X** denotes an unstable state in the heterogeneous nucleation phase transition process. In all subsequent analyses, we assume heterogeneous nucleation, following the Maxwell rule of phase transition.

5. Modes of actuation in laterally-constrained dielectric elastomers

We identify five modes of actuation (Table 1, Fig. 4). Modes-I, II, III and IV experience lateral loss of tension (Figs. 4a–c) and transit from a flat state (Fig. 2c) to a wrinkled state (Fig. 2e), but Mode-V remains in a flat state throughout the actuation process (Figs. 1c, 2c and 4d).

For the first four modes characterized by $\lambda_{2\text{p}}<\lambda_{\text{BI}}$, actuation response is differentiated by longitudinal pre-stretch ($\lambda_{1\text{p}}$). For $\lambda_{1\text{p}},\lambda_{2\text{p}}<\lambda_{\text{BI}}$ voltage increase beyond loss of tension causes expansion along λ_1 (Figs. 4a–c, all λ_{1p} except for $\lambda_{1p}=9$), while for $\lambda_{1\text{p}}>\lambda_{\text{BI}}$, $\lambda_{2\text{p}}>\lambda_{\text{BI}}$ an increase of voltage beyond loss of tension causes contraction along λ_1 (Figs. 4a–c, $\lambda_{1p}=9$). In both cases, the DE transits from a flat state to a wrinkled state. Transition to wrinkles is mediated by two processes – electromechanical instability leading to electromechanical phase transition, and lateral loss of tension. Here, we identify four modes of actuation, characterized by the type and order of appearance of the process that leads to wrinkles.

In Mode-I actuation, wrinkles appear as a result of two processes taking place simultaneously. This case is characterized by the super-charging voltage coinciding with the voltage causing lateral loss of tension ($\Phi_c=\Phi_w$). Fig. 3 illustrates this

transition based on the Maxwell rule. For Mode-I, the appearance of wrinkles take place gradually with increasing voltage, and stabilizes to a regular corrugated membrane at the conclusion of the transition (Fig. 2e), represented by state B of Figs. 2 and 3.

In Mode-II actuation, wrinkles appear as a result of lateral loss of tension only. In this mode, the electromechanical instability is fully suppressed, and the DE transits monotonically into a wrinkled state. Mode-II transition is signified by a sudden formation of regular corrugated wrinkles in the DE.

In Mode-III actuation, wrinkles first appear as a result of lateral loss of tension, followed by electromechanical instability. Mode-III transition may be characterized by a sudden appearance of regular corrugated wrinkles, followed by random transient wrinkles during electromechanical phase transition, ending with regular corrugated wrinkles.

In Mode-IV actuation, one may pre-stretch a DE such that $\lambda_{1p} > \lambda_{BI}$, leading to a Mode-II-like formation of wrinkles, followed by a contraction of the DE with increasing voltage. While the stretch decreases with increasing voltage, the charge on the membrane continues to increase, which is easily verified by plotting the equations in (2). This response is reminiscent of the human muscle and was mentioned in a previous work on uniaxial deformation (Huang and Suo, 2011). In this work, we observe this analytically in a laterally-constrained mode.

In Mode-V actuation, the lateral pre-stretch is larger than the limiting stretch for equal-biaxial deformation, $\lambda_{2p} > \lambda_{BI}$. The lateral stretch that is sufficient to realize Fig. 4d corresponds to the stretch limit for equal-biaxial deformation ($\lambda_{BI} = 8$ for $J_{lim} = 125$).

Fig. 5 plots maps of actuation modes on the $\lambda_{1p} - \lambda_{2p}$ plane, we shall ignore the contour relief on the plots for now (to be discussed in the following section) and focus on the boundaries and regions of actuation modes. We selected two values of J_{lim}: 125 and 50, which represents two common types of elastomers – acrylic and rubber, respectively (Kaltseis et al., 2014; Koh et al., 2011). For a given J_{lim}, we plot the curve $(\lambda_1^2 + \lambda_2^2 + \lambda_1^{-2}\lambda_2^{-2} - 3) = J_{lim}$ on the $\lambda_{1p} - \lambda_{2p}$ plane, to reveal a space of admissible pre-stretches. Mode-III is only possible for very small levels of λ_{2p}. For lateral pre-stretches smaller than $\lambda_{2p} = 5.8$ for $J_{lim} = 125$, and $\lambda_{2p} = 3.5$ for $J_{lim} = 50$, the DE actuates in either Mode-I or Mode-III, both of which are characterized by electromechanical instability leading to phase transition. For pre-stretches larger than $\lambda_{2p} = 5.8$ for $J_{lim} = 125$, and $\lambda_{2p} = 3.5$ for $J_{lim} = 50$, but smaller than $\lambda_{2p} = 8.0$ (the limit stretch in equal-biaxial), Mode-II and Mode-IV actuation dominates. Both modes are characterized by monotonic increase of actuation stretch with response to increase in voltage (for example Fig. 4c), with the sudden appearance of regular corrugated wrinkles due to lateral loss of tension only (2nd & 4th rows of Table 1). In Mode-II, the actuator continues to lengthen in the λ_1 direction after lateral loss of tension, while in Mode-IV, the actuator contracts after tension loss. Finally, for $\lambda_{2p} > 8.0$ in Figs. 5a and c (also illustrated in Fig. 4d), and $\lambda_{2p} > 5.2$ in Fig. 5b, the DE actuates purely in the flat state; lateral loss of tension will not take place. This is the classical plane strain deformation.

The varied actuation characteristics for a laterally-constrained DE may be attributed to one peculiar characteristic of a DE membrane – while one is free to mechanically deform the DE in any direction, deformation due to electric field always takes place in one direction through the thickness. In a laterally-constrained DE, the anisotropy of mechanical and electrical stresses gave rise to a plethora of actuation response. The theory presented in Sections 2–5, and the method to construct a map of actuation modes in Section 6, allows one to select appropriate combinations of pre-stretch for a laterally-constrained, for specific modes of actuation.

6. Actuation performance of a laterally-constrained dielectric elastomer

All analyses in the preceding sections ignore that a DE membrane may undergo dielectric breakdown when the electric field is excessive, preventing the DE membrane to actuate to its full potential of the limit stretch. Typical breakdown fields are in the order of 10^7 V/m for elastomeric materials (Pelrine et al., 2000; Gisby et al., 2013; Kaltseis et al., 2014; Zhao and Suo, 2007; Kollosche et al., 2012; Zhu et al., 2012; Huang et al., 2012; La and Lau, 2013). However, previous works on DE have shown that breakdown fields may be enhanced by various methods. In particular, pre-stretch may enhance the breakdown field by up to an order of magnitude to 10^8 V/m (Kaltseis et al., 2014; Kollosche et al., 2012; Zhu et al., 2012), and a DE membrane immersed in an electrically-inert fluid may further enhance the breakdown field close to 10^9 V/m (La and Lau, 2013). Analytically, one may express breakdown field (E_B) as a function of breakdown voltage (Φ_B) and stretches (λ_1, λ_2), as follows:

$$\frac{\Phi_B}{H} = E_B \lambda_1^{-1} \lambda_2^{-1} \tag{5}$$

Eq. (5) may similarly be specialized for all three modes of deformation. Specifically, we have:

$$\frac{\Phi_B}{H} = E_B \lambda^{-2} \tag{6a}$$

for equal-biaxial,

$$\frac{\Phi_B}{H} = E_B \lambda_1^{-1} \lambda_{2p}^{-1} \tag{6b}$$

for laterally-constrained, and

$$\frac{\Phi_B}{H} = E_B \lambda_1^{-1} \lambda_2^{-1} \tag{6c}$$

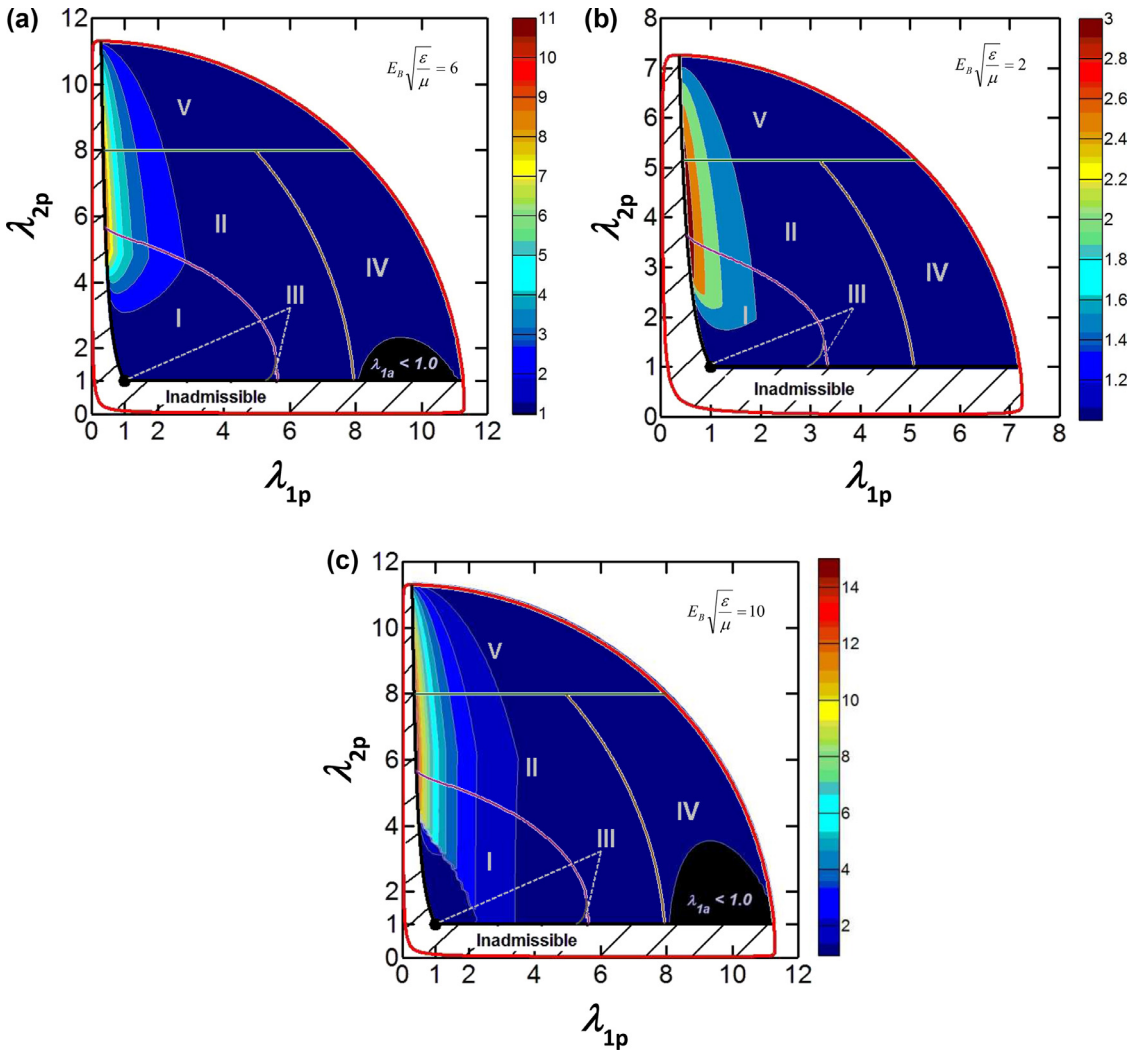

Fig. 5. Contour plots of maximum actuation on a λ_{1p}–λ_{2p} plane of a laterally-constrained actuator defined by its stretch limit $J_{\lim}$ and electromechanical strength $E_B\sqrt{\varepsilon/\mu}$. Each plot shows the maximum possible actuation stretch ($\lambda_{fail}/\lambda_{1p}$) for a combination of ($\lambda_{1p}$,$\lambda_{2p}$). Each plot takes on indicative material properties for (a) acrylic **VHB** elastomer; (b) natural rubber (**NR**); (c) a fictitious highly-stretchable, high-performance elastomer (**HP**). In all cases, actuation stretch is maximized when the DE evolves with a Mode-II electrically-induced actuation, with $\mathbf{P_{dead}}=0$. This inspires the design of freely-actuating DEs capable of very large continuously-tunable actuation.

for uniaxial, where λ_2 is related to λ_1 via setting $P_2=0$ in Eq. (2b).

Previous works have incorporated state-dependent E_B, for instance, E_B that varies with the state of stretch (Kaltseis et al., 2014; Huang et al., 2012), and E_B that varies with the small-strain shear stiffness (Kollosche et al., 2010). In our analysis which follows, we shall assume a fixed E_B independent from the state of the DE. This allows us to study the qualitative effect of an intrinsic value of E_B, on the maximum actuation of a laterally-constrained DE. One may be driven to incorporate state-dependent E_B to this analysis, which could be easily performed using methods presented in previous works (Koh et al., 2011; Huang et al., 2012). Nevertheless, we believe that while state-dependent E_B increases the complexity of analysis, it does not change the qualitative picture of maximum actuation.

Besides E_B, the material properties of small-strain shear stiffness μ, and dielectric permittivity ε, will also influence the performance of a DE actuator. A stiff elastomer will not actuate under an electric field significantly, while a dielectric with high permittivity encourages polarization, thereby enhancing the capability to actuate under an electric field. We non-dimensionalize Eq. (5) to give:

$$\frac{\Phi_B}{H}\sqrt{\frac{\varepsilon}{\mu}}=\left(E_B\sqrt{\frac{\varepsilon}{\mu}}\right)\lambda_1^{-1}\lambda_2^{-1} \tag{7}$$

Eq. (7) presents an electromechanical operating limit for a given DE. Again, we assume all material properties are independent of the state of the DE. The factor $E_B\sqrt{\varepsilon/\mu}$ on the right-hand-side of Eq. (7) provides a measure on the "electrome-

chanical strength" of the DE. A small value signals poor electromechanical performance, while a large value will indicate a good electromechanical performance.

We select three values of $E_B\sqrt{\varepsilon/\mu} = 2$, 6 and 10 for our illustration. The first two values of 2 and 6 correspond to typical material properties exhibited by natural rubber (Kaltseis et al., 2014; Treloar, 1975) and VHB (Pelrine et al., 2000; Kollosche et al., 2012; Zhu et al., 2012; Kollosche et al., 2010), respectively. The very large value of 10 is currently not commonly observed in typical elastomers. However, recent research have shown that it is possible to enhance the dielectric strength of VHB by 1.7 times, using silicone encapsulation (La and Lau, 2016; La and Lau, 2016), and that the dielectric constant of silicone-based rubbers may be improved by 1.5 times by the addition of carbon fibers (Subramani et al., 2014). Such a material currently does not exist, but we hope our analysis would spur the development of elastomers with high electromechanical strength.

Fig. 4 shows Eq. (7) superimposed on the voltage–stretch plane. The red solid lines indicate the maximum voltage before dielectric breakdown for a laterally-constrained DE (Eq. 6b), while the red dashed lines indicate the voltage limit for a uniaxially-deformed DE (Eq. 6c), representing that of a post-tension-loss laterally-constrained DE. For a small $E_B\sqrt{\varepsilon/\mu}$, the DE membrane always fails at very small actuation, like that of a piezoceramic. In this case, the actuation mode is irrelevant. Depending on the magnitude of $E_B\sqrt{\varepsilon/\mu}$, the DE in Mode-I and III may fail in one of the further three ways: First, it may fail at very small actuation, due to very small $E_B\sqrt{\varepsilon/\mu}$. Second, it may fail at the onset of instability and phase transition, as the material limit ($E_B\sqrt{\varepsilon/\mu}$) is not large enough for the DE to survive the full phase transition. This could be seen for example, the Mode-III actuation in Fig. 4a and 4b, for all values of $E_B\sqrt{\varepsilon/\mu}$, and several other examples for Mode-I in Figs. 4a and 4b. Third, it may fail after phase transition is complete, as could be seen for Mode-I in Fig. 4a and 4b, for $E_B\sqrt{\varepsilon/\mu} = 10$. The third way to fail allows for very large actuation. For Modes-II and IV, the magnitude of $E_B\sqrt{\varepsilon/\mu}$ only determines if the DE will fail in a flat (Fig. 4b for $E_B\sqrt{\varepsilon/\mu} = 2$, Fig. 4c for $E_B\sqrt{\varepsilon/\mu} = 2$ and 6) or wrinkled state (all others in Figs. 4a–c with failure dictated by intersection of dashed breakdown curves with the actuation curves). For Mode-V (Fig. 4d), the maximum actuation is simply the intersection of the actuation curve and the limit curve represented by $E_B\sqrt{\varepsilon/\mu}$. From Fig. 4c and 4d, it is further noted that the existence of a flat plateau of actuation curve provides a guide for a minimum $E_B\sqrt{\varepsilon/\mu}$ that enables the DE to undergo very large actuation. That minimum is such that $E_B\sqrt{\varepsilon/\mu}$ curve intersects at a point beyond the knee of the actuation curve, denoted by solid circles on Fig. 4c and 4d.

From Fig. 4, one may compute the maximum nominal actuation by reading the stretch at failure, λ_{fail}, indicated by crosses on Fig. 4a–c and 4d, where the limit line intersects the actuation response line. The total maximum actuation is λ_{fail}, normalized by the nominal stretch at zero voltage λ_{1p}, as follows:

$$\lambda_{1a} = \frac{\lambda_{fail}}{\lambda_{1p}} \tag{8}$$

As an example we consider $\lambda_{2p} = 9.0$ (Fig. 4d) for a material with high electromechanical limit $E_B\sqrt{\varepsilon/\mu} = 10$, with no dead load $P_{\text{dead}} = 0$ (left-most curve). The longitudinal stretch will vary between the pre-stretch $\lambda_{1p} = 9^{-0.5} = 0.333$ and the stretch at failure $\lambda_{fail} = 4.65$ hence $\lambda_{1a} = 14.0$ is the total maximum actuation. For a different mode of actuation e.g. Mode-I with $\lambda_{1p} = \lambda_{2p} = 3.0$ (Fig. 4b, second curve from the left) and electromechanical limit $E_B\sqrt{\varepsilon/\mu} = 2$ the stretch at failure is $\lambda_{fail} = 3.9$ hence $\lambda_{1a} = 1.3$.

Using representative material properties for the commonly-used acrylic elastomer VHB (Fig. 5a), natural rubber (Fig. 5b) and a high electromechanical strength material (Fig. 5c), we plot their actuation performance using contours. The maximum stretch at failure may either be read from a cross markers (for instance Fig. 4a–c), or the intersection of the material limit line and the actuation response curve (Fig. 4d). One may now scan the entire space of combinations of pre-stretches (λ_{1p}, λ_{2p}), assign specific limits governed by$E_B\sqrt{\varepsilon/\mu}$, and determine the maximum actuation the DE is capable of producing in accordance with Eq. (8). Fig. 5 shows a contour plot of maximum actuation, on the $\lambda_{1p} - \lambda_{2p}$ plane, superimposed on an actuation mode map. One may deduce from the plots, that actuation is maximized in Mode-II, for very small λ_{1p} (small P_{dead}). For very large pre-stretches in the λ_{1p} direction, coupled with small λ_{2p}, the DE undergoes a net contraction at maximum actuation ($\lambda_{1a} < 1.0$), as shown in Figs. 5a and 5c.

We further illustrate the actuation process on a force–stroke plane, as shown in Fig. 6. Plotting on this plane allows a user to determine how much stroke (actuation) the actuator may undergo when it carries a specific mechanical load (P_{dead}). To do this, we plot cross-sectional slices of Fig. 5, sliced at fixed values of λ_{2p}. We select cross-sections at $\lambda_{2p} = 1$, and at pre-stretches that optimize the maximum actuation, for instance, at $\lambda_{2p} = 6$ for $J_{\text{lim}} = 125$, and $\lambda_{2p} = 4$ for $J_{\text{lim}} = 50$. Here, we plot P_{dead} as the main ordinate (left vertical axis), and superimpose the equivalent λ_{1p} corresponding to P_{dead} as the supplementary ordinate (right vertical axis). From Eqs. (2a) and (3), λ_{1p} and P_{dead} is related as follows:

$$\frac{P_{\text{dead}}}{\mu L_2 H} = \frac{\lambda_{1p} - \lambda_{1p}^{-3}\lambda_{2p}^{-2}}{1 - \frac{\lambda_{1p}^2 + \lambda_{2p}^2 + \lambda_{1p}^{-2}\lambda_{2p}^{-2} - 3}{J_{\text{lim}}}} \tag{9}$$

Further, we express the actuation stroke in terms of percent strain (ε_{1a}), defined as:

$$\varepsilon_{1a} = 100(\lambda_{1a} - 1) \tag{10}$$

where λ_{1a} is given in (8). We thus use ε_{1a} to represent the actuation stroke. We create the force–stroke plane, as shown in Fig. 6. This plane shows the range of actuation strokes that is admissible when mechanical loads of varying magnitudes

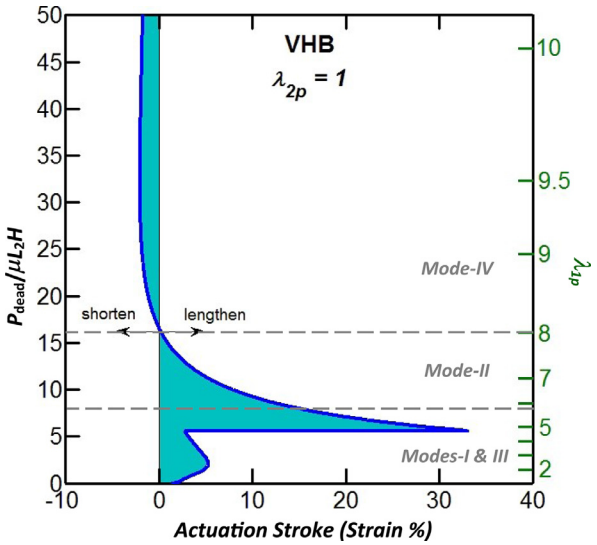

Fig. 6. The range of strokes that are accessible by electrical actuation (in % strain) using a fixed load $\mathbf{P_{dead}}$ for a laterally-constrained VHB dielectric elastomer with no lateral pre-stretch ($\lambda_{2p}=1.0$). For large $\mathbf{P_{dead}}$, the DE undergoes negative stroke – the DE shortens instead of lengthens under electrical actuation. The shaded region indicates all accessible strokes, and the boundary denotes the maximum achievable stroke.

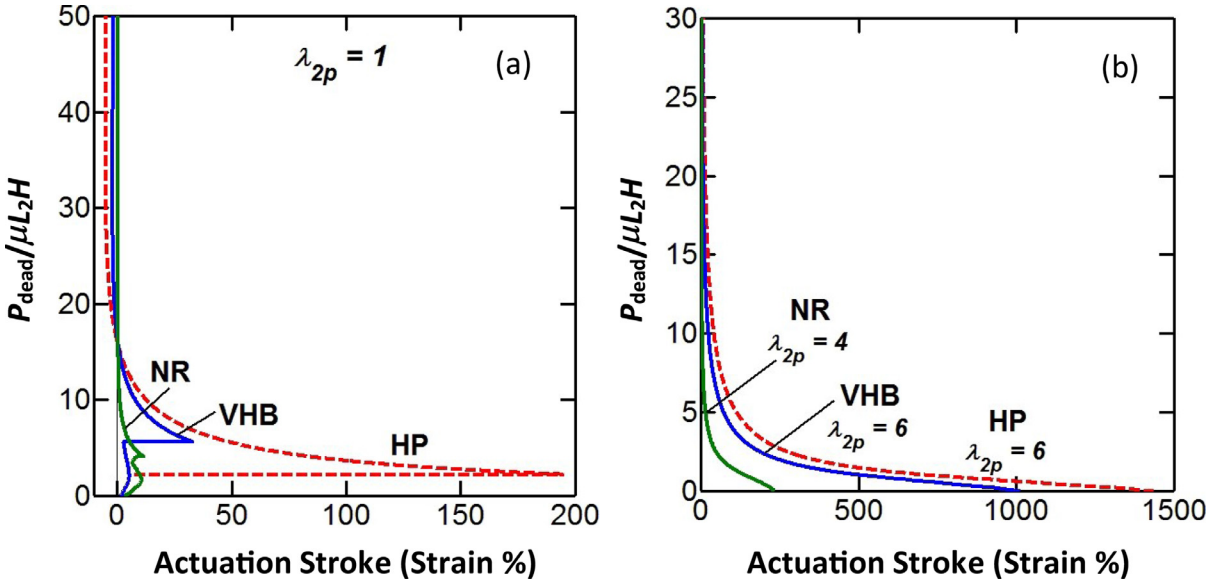

Fig. 7. Maximum stroke achievable by electrical actuation (in % strain) as a function of the applied fixed load P_{dead} for a laterally-constrained dielectric elastomer (a) clamped without lateral pre-stretch and (b) clamped with optimal lateral pre-stretch applied, for three different materials: Acrylic VHB elastomer (**VHB**), Natural Rubber (**NR**) and a high-performance material (**HP**) inspired by theoretical analysis.

(P_{dead}) are hung on the actuator. When the load is fixed, actuation paths of a horizontal line may be superimposed on the plot. One may also vary the load during actuation, and prescribe any arbitrary path on the plot. This plot may therefore be used as an aid in the design of actuators and their actuation pathways. Fig. 6 shows a force–stroke plot for $J_{\text{lim}} = 125$, at $\lambda_{2\text{p}} = 1$, for material limits of $E_B\sqrt{\varepsilon/\mu} = 6$, corresponding to a typical VHB elastomer.

Fig. 7 shows the force–stroke plots of three materials: VHB, Natural Rubber (NR) and the high-performance material (HP). These plots were plotted for various levels of lateral pre-stretches ($\lambda_{2\text{p}}$). For VHB and HP, $J_{\text{lim}} = 125$, while NR has $J_{\text{lim}} = 50$. Fig. 7a shows the force–stroke plot for $\lambda_{2\text{p}} = 1$. Fig. 7b shows lateral pre-stretch applied at a level where the maximum actuation stroke is expected to be a global maximum on the $\lambda_{1\text{p}} - \lambda_{2\text{p}}$ plane, which is $\lambda_{2\text{p}} = 6$ for $J_{\text{lim}} = 125$ (Figs. 5a and 5c for VHB and HP, respectively) and $\lambda_{2\text{p}} = 4$ (Fig. 5b for NR). We plot the cross-sectional slices on Fig. 7b. At this level of pre-stretch, only Mode-II and Mode-IV actuation is possible. However, Mode-IV actuation is extremely small at this level of pre-stretch; we left it out in our illustration. Hence, Fig. 7b only plots Mode-II actuation. Fig. 7b illustrates the possibility of actuating a free-standing DE (without the need to hang a mechanical load on the actuator) up to 230% for NR and

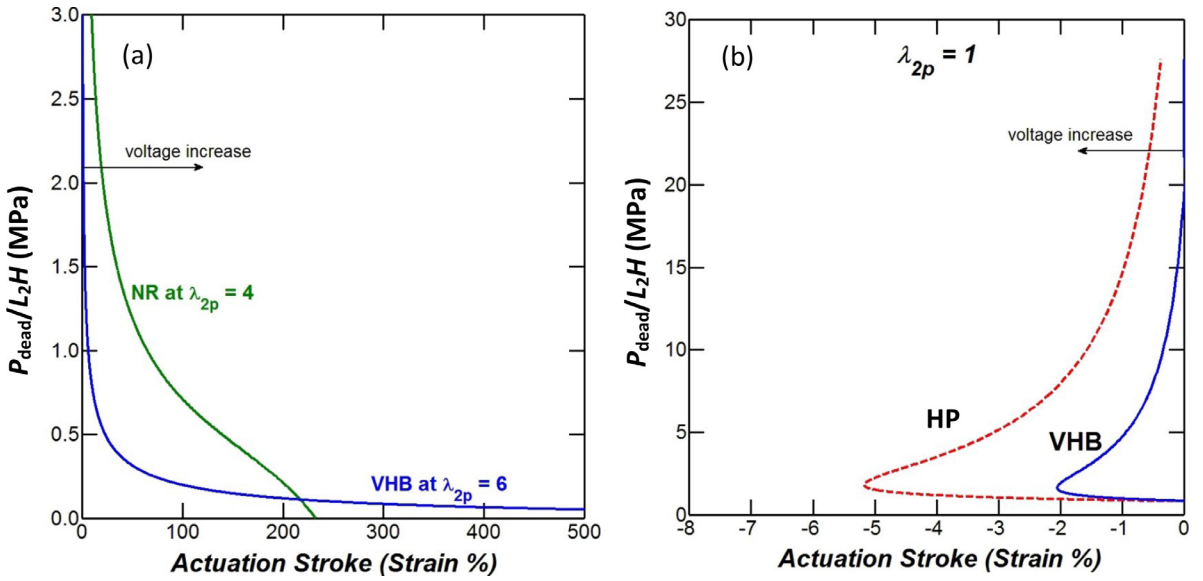

Fig. 8. The typical small-strain shear stiffnesses (μ) of acrylic elastomer (**VHB**) and natural rubber (**NR**) typically vary by about an order of magnitude. Here, we assume that $\mu_{\mathbf{VHB}} = 0.05$ MPa and $\mu_{\mathbf{NR}} = 0.5$ MPa. Fig. 7 is therefore re-plotted for both materials on a dimensional scale for the force axis in (a). Contractual actuation with increasing voltage is also plotted on a dimensional force scale in (b) for VHB and the high-performance elastomer (**HP**). Here, we assume that $\mu_{\mathbf{HP}} = 0.05$ MPa.

above 1000% for VHB. This theoretical observation motivates the possibility of developing free-standing, large-displacement actuators.

To facilitate design of experiments, we dimensionalize force to take units of nominal stress (MPa), as shown on Fig. 8. Fig. 8a illustrates very large actuation for VHB and NR. While VHB is able to actuate for a much larger stroke as compared with NR, NR is able to carry much larger loads, while sustaining a larger stroke than VHB. For instance, sustaining a nominal stress of 0.5 MPa (500 kPa), NR is able to attain a stroke of 130%, while VHB is only able to attain 20%. For reverse actuation as shown in Fig. 8b, the actuation is in general very small. Even for the high-performance material with an extremely high $E_B\sqrt{\varepsilon/\mu} = 10$, the maximum possible stroke is only 5%, resembling that of a stiff actuator. Hence, we may conclude that replicating the function of a contracting muscle with an electrical stimulus by a laterally-constrained dielectric elastomer, using Mode-IV actuation, will be largely ineffective.

7. Conclusion

This paper explores the modes of actuation in a laterally-constrained dielectric elastomer (DE), under all possible longitudinal and lateral pre-stretches, λ_{1p} and λ_{2p}. We show that a laterally-constrained actuator, of given pre-stretches and subject to an increasing electric field, can undergo various critical events, including electromechanical instability, wrinkling, and electrical breakdown. Depending on the sequence in which these critical events occur, we identify five modes of actuation, and locate them in the plane spanned by the values of the two pre-stretches, (λ_{1p}, λ_{2p}). To improve the range of actuation, one needs to exploit lateral pre-stretch, so that the DE actuates in the Mode-II region (Figs. 4 and 5). A laterally-constrained DE undergoes electromechanical instability and phase transition in Modes-I and III. While it is possible to suppress instability by longitudinal pre-stretch (λ_{1p}), the effectiveness of applying λ_{1p} on enhancing maximum actuation is significantly less than that by applying lateral pre-stretch (λ_{2p}). Our analysis has discovered possible giant actuation strokes, far exceeding the values previously reported for laterally-constrained actuators. We show that actuation stroke of beyond 1000% should be possible for a laterally-constrained, suitably pre-stretched acrylic VHB elastomer. It is also possible to achieve a 230% actuation stroke when natural rubber is suitably pre-stretched. This analysis opens the door to design actuators of simple geometry capable of a very large range of electromechanical actuation.

Acknowledgement

SJAK acknowledges the Ministry of Education - Singapore, FRC Tier 1 Funding, WBS No.: R-265-000-500-112, and the Agency for Science Technology and Research (A*STAR) IHPC-SMMI funding, WBS No.: R-265-000-488-305. Work performed by CK was supported by startup funds from the University of Colorado Boulder. CCF acknowledges the support by A*STAR SERC Grant No. 132 183 0025. RK, RB and SB acknowledge financial support from the European Research Council Advanced Investigators Grant SoftMap. ZS acknowledges the support of NSF work at Harvard is supported by MRSEC (DMR-0820484).

References

An, L., Wang, F., Cheng, S., Lu, T., Wang, T.J., 2015. Smart Mater. Struct. 24, 035006.
Böse, H., Fuβ, E., 2014. Proc. SPIE EAPAD 9056, 905614.
Carpi, F., Bauer, S., De Rossi, D., 2010. Science 330, 1759.
Carpi, F., De Rossi, D., 2005. IEEE Trans. Inf. Tech. Biomed. 9, 295.
Debenedetti, P.G., Stanley, H.E., 2003. Phys. Today 56, 40.
Gent, A.N., 1996. Rubber Chem. Tech. 69, 59.
Gisby, T.A., O'Brien, B.M., Anderson, I.A., 2013. Appl. Phys. Lett. 102, 193703.
Huang, J., Li, T., Foo, C.C., Zhu, J., Clarke, D.R., Suo, Z., 2012. Appl. Phys. Lett. 100, 041911.
Huang, J., Shian, S., Suo, Z., Clarke, D.R., 2013. Adv. Funct. Mater. 23, 5056.
Huang, J.S., Shian, S., Diebold, R.M., Suo, Z., Clarke, D., 2012. Appl. Phys. Lett. 101, 122905.
Huang, R., Suo, Z., 2011. Proc. Roy. Soc. A 468, 1014.
Kaltseis, R., Keplinger, C., Koh, S.J.A., Baumgartner, R., Goh, Y.F., Ng, W.H., Kogler, A., Tröls, A., Foo, C.C., Suo, Z., Bauer, S., 2014. RSC Adv. 4, 27905.
Kasahara, T., Mizushima, M., Shinohara, H., Obata, T., Futakuchi, T., Shoji, S., Mizuno, J., 2011. Jap. J. Appl. Phys. 50, 016502.
Keplinger, C., Li, T., Baumgartner, R., Suo, Z., Bauer, S., 2012. Soft Matter 8, 285.
Kim, D., Lee, C.H., Kim, B.C., Lee, D.H., Lee, H.S., Nguyen, C.T., Kim, U.K., Nguyen, T.D., Moon, H., Koo, J.C., Nam, J., Choi, H.R., 2013. Proc. SPIE EAPAD 8687, 86872J.
Koh, S.J.A., 2009. MRS Proc. 1218, Z7–10.
Koh, S.J.A., Keplinger, C., Li, T., Bauer, S., Suo, Z., 2011. IEEE. Trans. Mech. 16, 33.
Koh, S.J.A., Li, T., Zhou, J., Zhao, X., Hong, W., Zhu, J., Suo, Z., 2011. J. Polym. Phys. B 49, 504.
Koh, S.J.A., Zhao, X., Suo, Z., 2009. Appl. Phys. Lett. 94, 262902.
Kollosche, M., Kofod, G., Suo, Z., Zhu, J., 2015. J. Mech. Phys. Solids 76, 47.
Kollosche, M., Stoyanov, H., Ragusch, H., Risse, S., Becker, A., Kofod, G., 2010. Electrical breakdown in soft elastomers: stiffness dependence in un-pre-stretched elastomers. In: Proc. IEEE Int. Conf. Solid Dielectrics (ICSD).
Kollosche, M., Zhu, J., Suo, Z., Kofod, G., 2012. Phys. Rev. E 85, 051801.
La, T.G., Lau, G.K., 2013. Appl. Phys. Lett. 102, 192905.
La, T.G., Lau, G.K., 2016. Enhanced Dielectric Strength and Actuation of Acrylic Elastomer with Silicone Gel Coating. In: Proceedings of SPIE, 9798, pp. 97980D–979801.
La, T.G., Lau, G.K., 2016. Appl. Phys. Lett. 108, 012903.
Laflamme, S., Kollosche, M., Connor, J.J., Kofod, G., 2013. J. Eng. Mech. 139, 879.
Lu, T., Foo, C.C., Huang, J., Zhu, J., Suo, Z., 2014. J. Appl. Phys. 115, 184105.
McKay, T.G., O'Brien, B., Calius, E., Anderson, I., 2010. Smart Mater. Struct. 19, 055025.
McKay, T.G., Rosset, S., Anderson, I.A., Shea, H., 2015. Smart Mater. Struct. 24, 015014.
Pelrine, R., Kornbluh, R., Pei, Q., Joseph, J., 2000. Science 287, 836.
Pelrine, R., Kornbluh, R.D., Eckerle, J., Jeuck, P., Oh, S., Pei, Q., Stanford, S., 2001. Proc. of SPIE 4329, 148.
Plante, J., Dubowsky, S., 2007. Sens. Actuators A 137, 96.
Pruppacher, H.R., Klett, J.D., 2010. Microphysics of Clouds and Precipitation. Springer, Dordrecht Heidelberg London New York, pp. 191–209. Chapter 7.
Subramani, K.B., Cakmak, E., Spontak, R.J., Ghosh, T.K., 2014. Adv. Mater. 26, 2949.
Suo, Z., 2010. Acta Mechanica Solida Sinica 23, 549.
Treloar, L.R.G., 1975. Physics of Rubber Elasticity. Clarendon Press, Oxford, pp. 81–100. Chapter 5.
Zhao, X., Hong, W., Suo, Z., 2007. Phys. Rev. B 76, 134113.
Zhao, X., Suo, Z., 2007. Appl. Phys. Lett. 91, 061921.
Zhu, J., Kollosche, M., Lu, T., Kofod, G., Suo, Z., 2012. Soft Matter 8, 8840.